

# Propagation of non-linear circularly polarised Alfvén waves in a homogeneous medium

Rim Turkmani <sup>\*</sup> and Ulf Torkelsson

Chalmers University of Technology/Göteborg University, Department of Astronomy & Astrophysics,  
S-412 96 Gothenburg, Sweden

Accepted 23-07-03

**Abstract.** We study the evolution of non-linear circularly polarised Alfvén waves by solving numerically the time-dependent equations of magnetohydrodynamics (MHD) in one dimension. We examine the behaviour of the waves and find that different physical mechanisms are relevant in different ranges of  $\beta$ . In a low  $\beta$  plasma the wave may undergo a parametric decay. This is because the wave excites a density enhancement that travels slower than the wave itself and thus interacts with the wave. When  $\beta \geq 1$  the density enhancement does not interact with the wave and no decay takes place, instead the Alfvén wave is reflected against the density enhancement. The reflection zone propagates with the speed  $\frac{1}{n}v_A$ . Because of that the magnetic flux is conserved which results in an amplification of the oscillating magnetic field by a factor  $\frac{1}{n}$ . We find that  $n$  depends on  $\beta$ , and that in particular it is  $\leq 1$  for values of  $\beta \sim 1$  and  $\geq 1$  for  $\beta \gg 1$ . We discuss the relevance of these mechanisms to the acceleration of the solar wind, and the triggering of MHD turbulence in the polar wind region. In particular these simulations can explain the presence of inward propagating Alfvén waves in the solar corona.

**Key words.** MHD – waves – solar wind – stars : mass-loss.

## 1. Introduction

The expanding coronal model proposed by Parker (1958) predicted the existence of the solar wind. Observations by space probes showed later that there are two forms of solar wind: the slow solar wind (up to 400 km/s) which fits the Parker model, and the fast solar wind (up to 800 km/s) which emanates from the coronal holes, regions in the solar corona with open magnetic field lines and low density.

Large amplitude, low frequency, Alfvén waves have been observed in the solar corona for over 30 years (e.g. Belcher & Davis 1971). During the last decade Ulysses has provided plasma and magnetic field measurements that have allowed extensive investigations of the behaviour of Alfvénic turbulence in the high-latitude solar wind. The data shows a strong correlation between the fluctuations in velocity and magnetic fields (Smith et al. 1995), and revealed the presence of both inward and outward directed Alfvén waves (e.g. Bavassano et al. 2000). While the outward going waves are expected to be generated at the coronal base, the source of the inward going waves in the solar wind is not yet understood.

Alfvén waves play a crucial role in several models for the acceleration of the fast solar wind (e.g. Leer et al.

1982). An attractive feature of the Alfvén waves is that they can propagate over vast distances since they are incompressible to lowest order, and therefore do not dissipate easily. However, dissipative damping is required at some point to avoid too high wind velocities (e.g. Holzer et al. 1983).

In two dimensions phase mixing due to a transverse gradient in the phase velocity (e.g. Heyvaerts & Priest 1983) can lead to a strong damping of the wave. This mechanism is not available in one dimension though, and one has then rather to consider the nonlinear coupling of the Alfvén wave with other modes (e.g. Wentzel 1973). A close examination of the properties of Alfvén waves shows that a linearly polarised Alfvén wave is compressible to second order though, because the magnetic pressure,  $B_{\perp}^2/2\mu_0$ , is modulated on half the wave length of the Alfvén wave itself (Alfvén & Fälthammar 1963). This opens up the possibility that a high-amplitude Alfvén wave can steepen, which was demonstrated analytically by Cohen & Kulsrud (1974). As the wave steepens, it forms current sheets at the nodes of the fluctuating magnetic field. This effect has been studied in numerical simulations by Boynton & Torkelsson (1996) and Ofman & Davila (1997).

In a circularly polarised Alfvén wave, on the other hand, the magnetic pressure is constant along the wave, which is the physical reason why it is an exact solution

<sup>\*</sup> Present address: Space and Atmospheric Physics, The Blackett Laboratory, Imperial College, London, England.

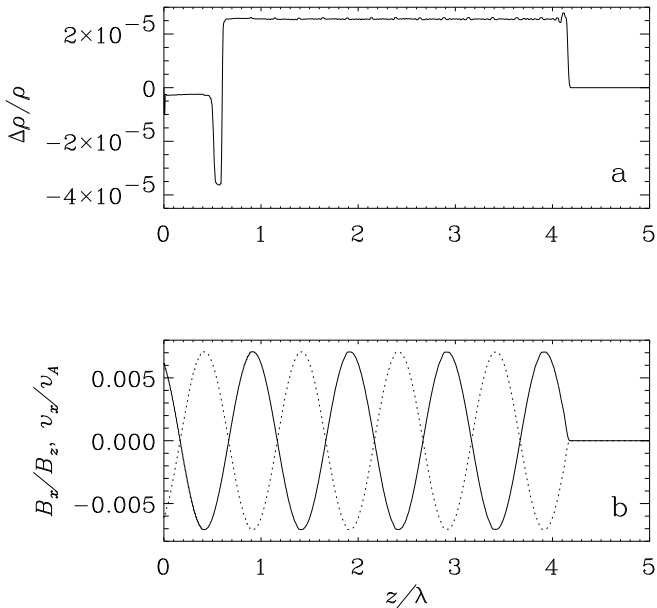


**Fig. 1.** Low amplitude magnetohydrodynamic waves propagating through a homogeneous medium of low  $\beta$  (Run 1a). **a**  $\Delta\rho/\rho = \frac{\rho - \rho_0}{\rho_0}$  versus  $z/\lambda$  at  $t/P = 4.2$ . **b**  $B_x/B_z$  (solid line) and  $v_x/v_A$  (dotted line) versus  $z/\lambda$  at the same time.

of the nonlinear MHD equations. However, the wave can still decay via a parametric instability (e.g. Sagdeev & Galeev 1969), which is usually less important than the wave steepening for a linearly polarised Alfvén wave. In this instability a forward propagating Alfvén wave in the presence of a density fluctuation generates a forward propagating acoustic wave and a backward propagating Alfvén wave.

Parametric decay has many applications in plasma physics and astrophysics. In coronal physics it has been proposed to be a possible mechanism to trigger MHD turbulence in regions with relatively smooth density profiles like the polar wind region and to account for the small compressible fluctuations in the solar wind (Goldstein 1978). It is also a candidate for generating the inward propagating Alfvén waves in the solar wind (e.g. Tu & Marsch 1989)

The parametric decay of circularly polarised Alfvén waves has been studied both analytically (e.g. Cohen 1975, Derby 1978, Goldstein 1978, Jayanti & Hollweg 1993) and numerically by several groups (e.g. Del Zanna et al. 2001, Malara et al. 2000, Pruneti & Velli 1997, Ghosh & Goldstein 1994, Ghosh et al. 1994, Umeki & Terasawa 1992). Except for the work by Pruneti & Velli (1997) these studies have been restricted to Alfvén waves in homogeneous media. Most of these numerical simulations have studied how Alfvén waves of different frequencies interact and generate turbulence, and determine the properties of fully developed turbulence. For these purposes it is appropriate to use a model with periodic boundary conditions

and introduce Alfvén waves that extend over the entire grid through the initial state (Malara et al. 2000 and Del Zanna et al. 2001).

On the contrary we will study how a *fresh* Alfvén wave falls prey to the parametric instability, which gradually converts it into a backward propagating Alfvén wave and an acoustic wave. To do this we drive the Alfvén wave on one of the boundaries of our model. Since there is no Alfvén wave in the interior initially we are able to study how processes at the propagating wave front eventually lead to the breakdown of the entire Alfvén wave further upstream, a phenomenon that cannot be found using periodic boundary conditions. Our approach is similar to that of Boynton & Torkelsson (1996), who studied linearly polarised Alfvén waves. Since the processes that we study occur gradually it is important to use a grid that extends over many wave lengths to capture them, which limits us to using a one-dimensional model. The need for an very extended grid becomes clear if one compares the works by Torkelsson & Boynton (1998) and Ofman & Davila (1997). Torkelsson & Boynton found a much stronger damping in their one-dimensional model than Ofman & Davila did in their two-dimensional model, but most of the damping occurred beyond the outer boundary of the Ofman & Davila model.

A highly simplified numerical model such as the one that we present in this paper cannot provide a realistic representation of the physics of Alfvén waves in the solar wind, however it can still be useful since it allows us to study a limited number of physical processes in detail. The understanding that we gain from this can then serve as a guide in interpreting some aspects of more complex numerical simulations, such as the ones carried out by Tsiklauri et al. (2002) and Tsiklauri & Nakariakov (2002) and Laveder et al. (2002a, 2002b).

The plan of the paper is the following: In Sec. 2 we describe the basic MHD equations and review the properties of the parametric decay. Our models and results are presented in Sect. 3. We discuss how the results relate to the dynamics of Alfvén waves in the solar wind in Sect. 4 and we summarise our conclusions in Sect. 5.

## 2. Mathematical formulation

### 2.1. Fundamental properties of Alfvén waves

The equations of ideal isothermal MHD in a homogeneous medium can be written as

$$\frac{\partial \rho}{\partial t} + \nabla \cdot (\rho \mathbf{v}) = 0, \quad (1)$$

$$\frac{\partial(\rho \mathbf{v})}{\partial t} + \nabla \cdot (\mathbf{v} \rho \mathbf{v}) = -\nabla p + \mathbf{J} \times \mathbf{B}, \quad (2)$$

$$\frac{\partial \mathbf{B}}{\partial t} = \nabla \times (\mathbf{v} \times \mathbf{B}), \quad (3)$$

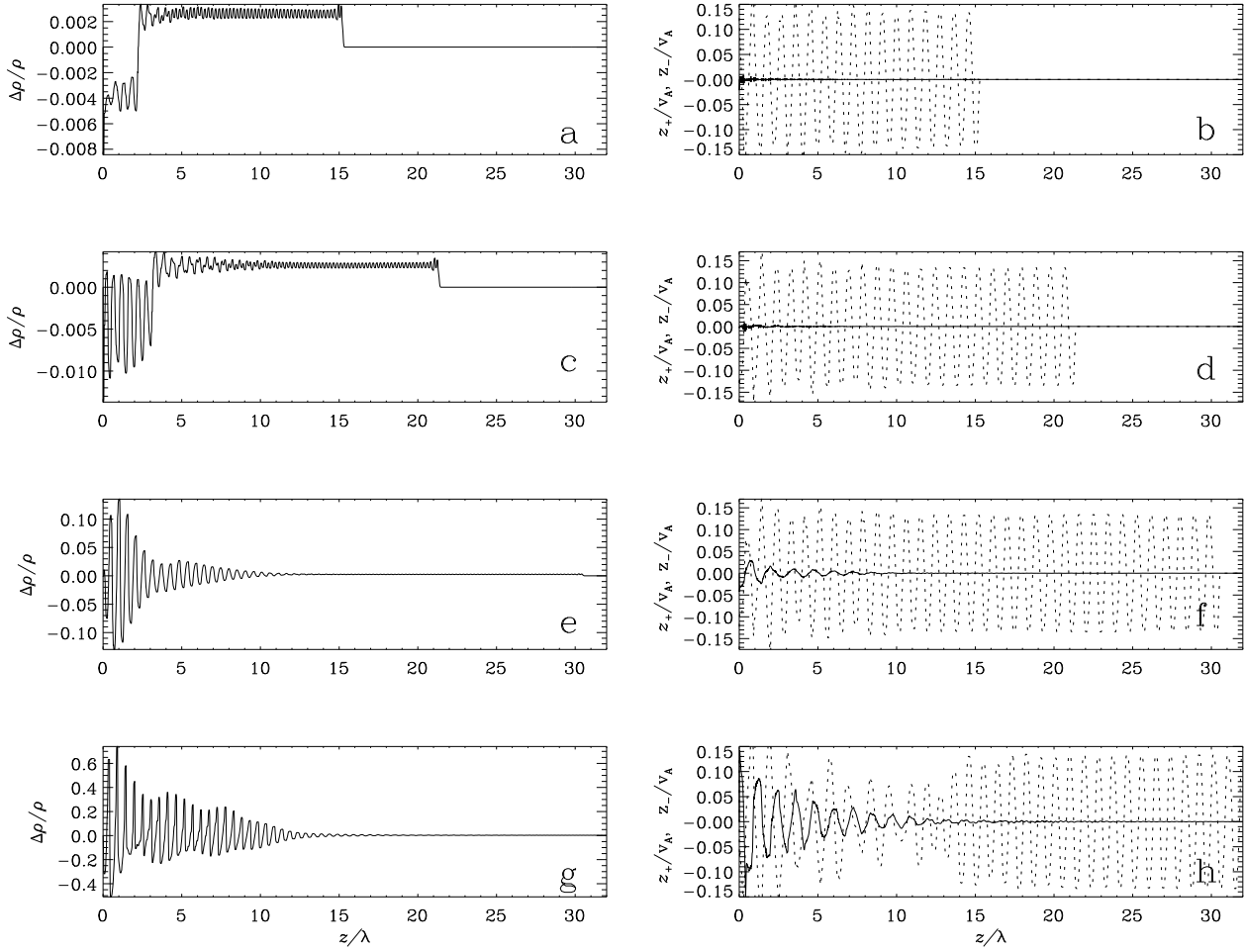


**Fig. 2.** Magnetohydrodynamic waves propagating through a homogeneous medium of low  $\beta$  and  $\eta = 0.07$  (Run 1b). **a, c, e, g**  $\Delta\rho/\rho = \frac{\rho - \rho_0}{\rho_0}$  versus  $z/\lambda$  at  $t/P = 16.7, 23.3, 33.3, 46.7$ . Note the changes in the  $\Delta\rho/\rho$ -scale between the frames. **b, d, f, h**  $z_-/v_A$  (solid line) and  $z_+/v_A$  (dotted line) versus  $z/\lambda$  at the same times.

$$\nabla \cdot \mathbf{B} = 0, \quad (4)$$

where  $\rho$  is the density,  $\mathbf{v}$  the velocity,  $p$  the pressure,  $\mathbf{B}$  the magnetic field, and  $\mathbf{J} = \nabla \times \mathbf{B}/\mu_0$  the current density. Eqs. (1) and (2) express the conservation of mass and momentum, respectively, and Eq. (3) is the induction equation. The constraint  $\nabla \cdot \mathbf{B} = 0$  is fulfilled by Eq. (3) if it is imposed as an initial condition. For fully ionised hydrogen we can write the equation of state as

$$p = \frac{2\rho k_B T}{m_H}, \quad (5)$$

where  $k_B$  is Boltzmann's constant,  $T$  the temperature and  $m_H$  the mass of the hydrogen atom.

In a homogeneous medium with a density  $\rho_0$  and a background magnetic field  $\mathbf{B} = B_z \hat{\mathbf{z}}$  a circularly polarised forward propagating Alfvén wave is described by the transverse magnetic field

$$\mathbf{B}_\perp = B_\perp [\cos(kz - \omega t)\hat{\mathbf{x}} + \sin(kz - \omega t)\hat{\mathbf{y}}], \quad (6)$$

and the velocity

$$\mathbf{v}_\perp = -\frac{\mathbf{B}_\perp}{\sqrt{\mu_0 \rho_0}}, \quad (7)$$

while for a backward propagating Alfvén wave the velocity is given by

$$\mathbf{v}_\perp = \frac{\mathbf{B}_\perp}{\sqrt{\mu_0 \rho_0}}. \quad (8)$$

In both cases the Alfvén wave obeys the dispersion relation

$$\omega = v_A k \quad (9)$$

with the Alfvén velocity

$$v_A = \frac{B_z}{\sqrt{\mu_0 \rho_0}}. \quad (10)$$

In order to separate forward and backward propagating Alfvén waves it is useful to introduce the Elsässer variables

$$Z_\pm = \left| \mathbf{v}_\perp \mp \frac{\mathbf{B}_\perp}{\sqrt{\mu_0 \rho}} \right|, \quad (11)$$

**Table 1.** Simulations of Alfvén waves in a homogeneous medium. The wave is characterised by the two quantities  $\eta$ , the amplitude of the imposed Alfvén wave in terms of the vertical magnetic field, and  $\beta = 2\mu_0 p/B_z^2$  the plasma beta. For the different Runs we further specify the length of the time step  $\Delta t$  in terms of the period of the wave,  $P$ , the length of the computational domain,  $L$  in terms of the wave length,  $\lambda$ , and the number of grid points,  $N$ .

Run	$\Delta t/P$	$N$	$L/\lambda$	$\eta$	$\beta$
1a	0.003 3	3 600	78	0.007	0.042
1b	0.003 3	3 600	78	0.07	0.042
1c	0.003 3	3 600	78	0.7	0.042
2a	0.003 3	13 500	193	0.007	0.96
2b	0.003 3	13 500	193	0.07	0.96
2c	0.003 3	13 500	193	0.7	0.96
3a	0.003 3	13 500	278	0.007	2
3b	0.003 3	13 500	278	0.007	2
3c	0.003 3	13 500	278	0.07	2
4a	0.001 7	36 000	77.2	0.007	17
4b	0.001 7	36 000	77.2	0.07	17
4c	0.001 7	36 000	77.2	0.7	17

which describe the forward and backward propagating Alfvén waves, respectively. For a pure forward propagating Alfvén wave  $z_-$  does not exist while  $z_+$  has twice the value of  $v_\perp$  of the original wave. For the circularly polarised wave the magnetic pressure  $B_\perp^2/(2\mu_0)$  is the same everywhere inside the wave. This is the physical reason why an infinitely extended circularly polarised Alfvén wave is incompressible and an exact solution of the nonlinear MHD equations, whereas the linearly polarised wave

$$\mathbf{B}_\perp = B_\perp [\cos(kz - \omega t)\hat{\mathbf{x}} + \cos(kz - \omega t)\hat{\mathbf{y}}], \quad (12)$$

is compressible to second order, and therefore not an exact solution of the nonlinear MHD equations.

In the one-dimensional problem that we study, there is only one additional wave mode, an acoustic wave obeying the dispersion relation

$$\omega = c_s k, \quad (13)$$

where the isothermal speed of sound is

$$c_s = \sqrt{\frac{p_0}{\rho_0}}. \quad (14)$$

The amplitude of the density oscillation  $\Delta\rho = \rho - \rho_0$  is related to that of the longitudinal velocity,  $v_z$ , through

$$v_z = \frac{\Delta\rho}{\rho} c_s \quad (15)$$

(e.g. Landau & Lifshitz 1987).

## 2.2. Parametric decay

In the presence of a density fluctuation a circularly polarised Alfvén wave decays into forward propagating density and magnetic waves in addition to a backward propagating magnetic wave. These waves are not necessarily normal modes of the plasma.

Galeev & Oraevskii (1963) and Sagdeev & Galeev (1969) showed that an Alfvén wave with a frequency  $\omega_0 = v_A k_0$  and a wave number  $k_0$  can decay into a backward propagating Alfvén wave with a frequency  $\omega_-$  and a wave number  $k_-$  and a forward propagating acoustic wave with a frequency  $\omega$  and a wave number  $k$  that fulfill the resonance conditions

$$\omega_0 = \omega + |\omega_-| \quad (16)$$

and

$$k_0 = k - k_- \quad (17)$$

(e.g. Cramer 2001).

Goldstein (1978) and Derby (1978) derived the dispersion relation for low frequency waves neglecting dispersive effects

$$\begin{aligned} (\omega^2 - c_s^2 k^2)(\omega - v_A k)[(\omega + v_A k)^2 - 4\omega_0^2] \\ = \frac{\eta v_A^2 k^2}{2} [\omega^3 + \omega^2 v_A k - 3\omega\omega_0^2 + \omega_0^2 v_A k] \end{aligned} \quad (18)$$

where  $\eta = \frac{B_\perp}{B_z}$ . In the limit of  $\beta \ll 1$  Eq. (18) yields a maximum growth rate for the instability near  $k \simeq 2k_0$  for the density wave. The backward propagating magnetic wave has then  $\omega_- \simeq -\omega_0$  and  $k_- \simeq k_0$  resulting in  $\omega_- \simeq -v_A k_-$ . This means that it is a natural mode of the system, an Alfvén wave, and at the same time the forward propagating density wave is an acoustic wave. In this regime we therefore obtain a parametric instability. When  $\beta$  increases the daughter wave becomes less resonant with the normal mode and the modulational instability loses its parametric nature.

## 3. Results

We use the numerical code of Boynton & Torkelsson (1996) to simulate circularly polarised Alfvén waves. This code is based on the ETBFCT algorithm (Boris 1976), a form of flux-corrected transport (Boris & Book 1973). The scheme is fairly inefficient compared to modern methods; it needs about 30 to 40 grid points per wave length of the Alfvén wave, while there are schemes that require only a third of this. However the memory and time requirements for a one-dimensional simulation are sufficiently small that this is acceptable.

The waves are driven on the lower boundary of a one-dimensional box and propagate through a homogeneous medium. In all the runs the grid is sufficiently extended that the wave does not hit the upper boundary during the course of the simulation. The lower boundary condition is formulated in such a way that it only allows an outward propagating Alfvén wave. This can be a problem since backward propagating Alfvén waves are generated in the simulations. These are mostly of low amplitude though, and it is only very late in the simulations that high-amplitude Alfvén waves reach the lower boundary,

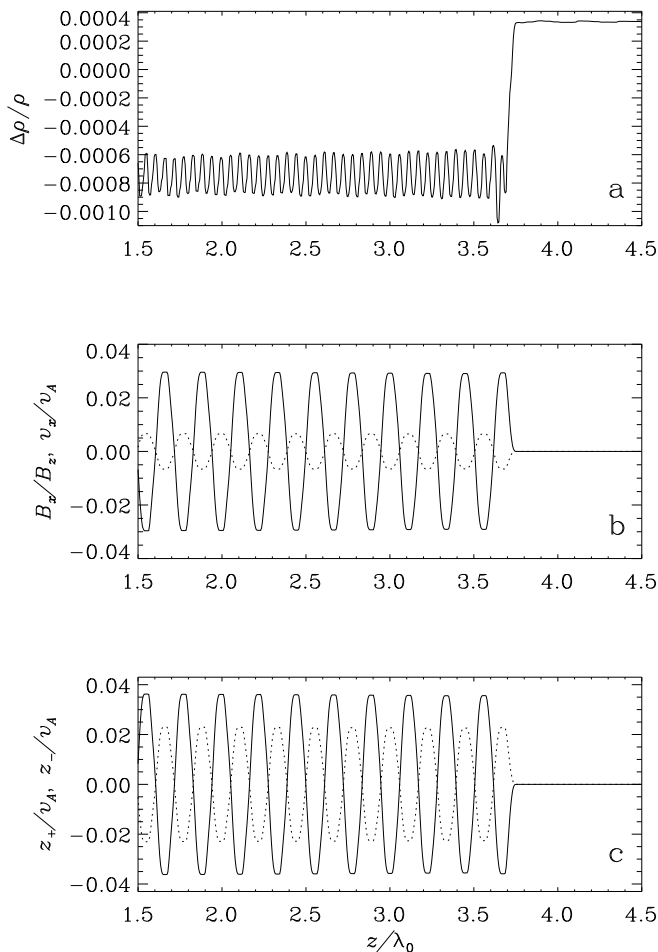


**Fig. 3.** Magnetohydrodynamic waves propagating through a homogeneous medium of  $\beta = 0.96$  and  $\eta = 0.007$  (Run 2a). **a**  $\Delta\rho/\rho = \frac{\rho - \rho_0}{\rho_0}$  versus  $z/\lambda_0$  at  $t/P = 16.7$ . **b**  $B_x/B_z$  (solid line) and  $v_x/v_A$  (dotted line) versus  $z/\lambda_0$  at the same time. **c**  $z_+/v_A$  (solid line),  $z_-/v_A$  (dotted line) as versus  $z/\lambda_0$  at the same time.

and the physical processes that we are interested in occur far from the boundary then.

We study waves of different amplitudes,  $\eta$ , at different values of  $\beta$ , the ratio of gas pressure to magnetic pressure (Tab. 1). The magnetic field is strong in runs 1a-c, that is  $v_A > c_s$ , intermediate in runs 2a-c and 3a-c, that is  $v_A \sim c_s$  and weak in runs 4a-c, that is  $c_s > v_A$ .

### 3.1. Very low $\beta$

As an example we look at run 1a ( $\beta = 0.042$ ) with a strong magnetic field and a low-amplitude Alfvén wave ( $\eta = 0.007$ ). The propagating wave is shown in Fig. 1b. The Alfvén wave excites a density enhancement (Fig. 1a), whose right edge coincides with the front of the Alfvén wave, while the left edge propagates with the lower speed  $c_s$ . This density enhancement is a second order effect, and its amplitude is consequently proportional to the square of

the amplitude of the Alfvén wave. One should note here that for a linearly polarised wave the corresponding enhancement shows a strong sinusoidal modulation (1996).

The density discontinuity at the front of the Alfvén wave excites a secondary compressional wave which becomes more pronounced for the higher amplitude run 1b ( $\eta = 0.07$ ). This wave can be seen as a weak modulation of the density enhancement (Figs. 1a, 2a), and also of the magnetic pressure  $|\mathbf{B}_\perp|^2/(2\mu_0)$ . The density peaks coincide with the peaks of the magnetic pressure making them a third order analogue of the fluctuations found by Boynton & Torkelsson (1996, Fig. 2a).

The density fluctuations serve as the necessary seeds of the parametric instability, but due to the low amplitude of the fluctuations the instability grows slowly. The evolution of the backward-propagating Alfvén wave that is generated by the instability can be followed in Figs. 2b, d, f and h. It grows in amplitude away from the wave front, which enhances the growth rate of the parametric instability upstream. Eventually, the instability is so strong that it becomes an efficient source of a forward-propagating sound wave (Figs. 2a, c, e and g). We get a region at  $z < 15\lambda_0$  in Fig. 2g and h, in which the waves are strongly interacting. In this region there is a strong damping of the forward-propagating Alfvén wave, and the acoustic wave is amplified until it becomes so nonlinear that it steepens into shocks. On the other hand since the Alfvén speed is larger than the sound speed, the head of the Alfvén wave manages to stay ahead of the density fluctuations and therefore remains essentially unaffected by the parametric decay.

In agreement with the theoretical prediction the sound wave has a wave number  $k \simeq 2k_0$ . Figures 2d and f show that there is a phase shift of  $\frac{\pi}{2}$  between the backward- and the forward-propagating Alfvén waves as we expect if the backward-propagating wave is generated through the parametric instability.

### 3.2. $\beta = 0.96$ and 2

We look first at the low amplitude wave 2a. The Alfvén wave is reflected against a density enhancement at the front of the Alfvén wave (Fig. 3a and c). The density enhancement acts like a wall that is pushed to the right by the wave. Fig. 3c shows that the reflected wave, represented by  $z_-$ , has a phase shift of  $\pi$  radians relative to the mother wave, which is characteristic of reflection at a fixed end. To the left of the density enhancement (Fig. 3a) we see rapid fluctuations in the density (cf. the low  $\beta$  models).

The right edge of the density enhancement travels at a speed  $\simeq c_s + v_z$  as expected from an acoustic wave, while the left edge of the density enhancement, that is the front of the Alfvén wave, travels at  $v_f = 0.23 v_A = v_A/n$ . As a consequence of this, the measured wave length of the Alfvén wave is  $\lambda_0/n = 0.23 \lambda_0$ , where  $\lambda_0 = v_A P$ . We can see also that the wave does not show the ordinary re-

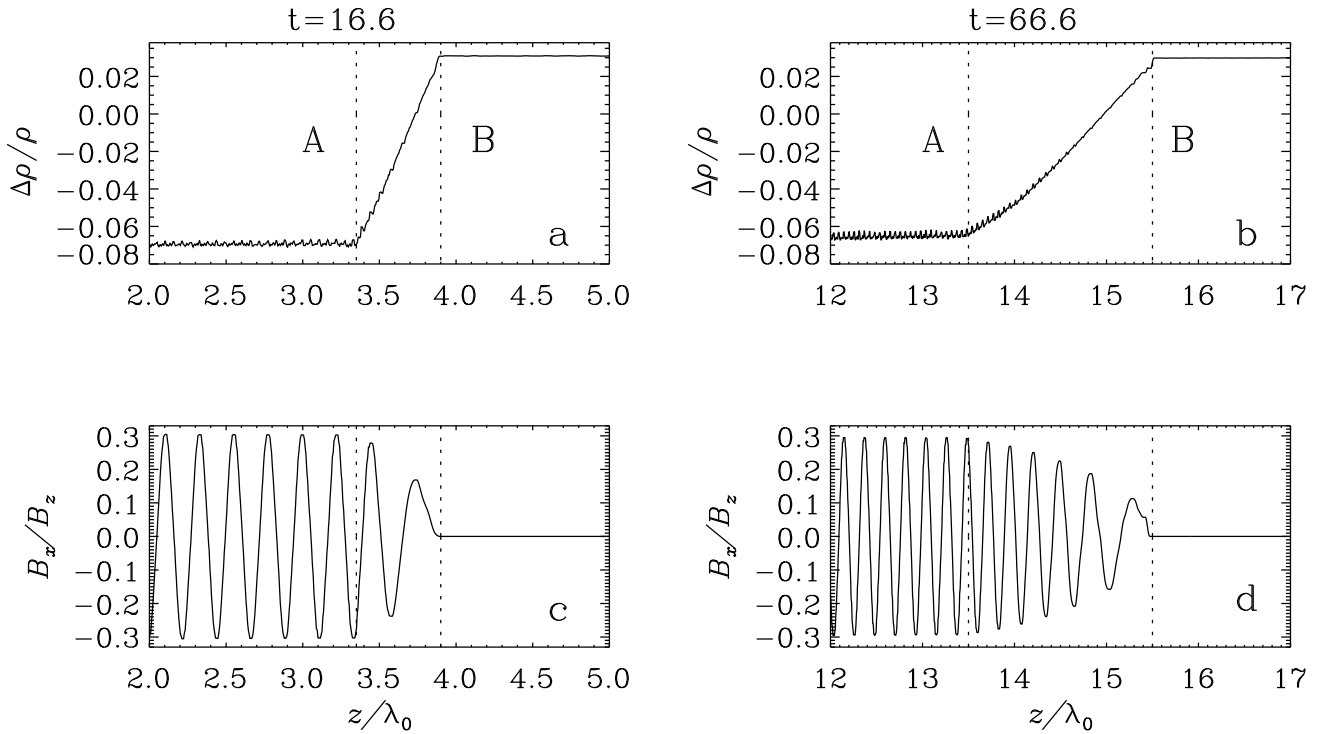


**Fig. 4.** Magnetohydrodynamic waves propagating through a homogeneous medium of  $\beta = 0.96$  and  $\eta = 0.07$  (Run 2b). The plots focus on the Alfvén wave front at two times,  $16.6P$  (**a**, **c**) and  $66.6P$  (**b**, **d**). The upper panels **a** and **b** show  $\Delta\rho/\rho$  versus  $z/\lambda_0$ , while the lower panels **c** and **d** show  $B_x/B_z$  versus  $z/\lambda_0$ .

lation between  $v_x$  and  $B_x$  that we expect for an Alfvén wave (Fig. 3b). While the transverse velocity component maintain the relation  $v_x/v_A = \eta$  we find for the fluctuating magnetic field  $B_x/B_z = 4.25\eta = n\eta$ . This can be easily understood. During half a period the injected flux of the  $x$ -component of the magnetic field is  $\eta v_A B_z P/\pi$ , but because the wave propagates at the speed  $v_A/n$ , this magnetic flux is compressed into a distance  $v_A P/n$ , which leads to that the magnetic field is amplified by the factor  $n$ .

The dynamics of the reflection zone is more easily studied in a wave with a higher amplitude, because the extent of the reflection zone increases with the amplitude of the wave. We show the reflection zone of model 2b at two different times in Fig. 4. The density changes smoothly along a positive slope between the positions A and B. The slope becomes less steep with time since it is spreading out over a longer distance. To the left of A the phase speed  $v_p = \lambda/P = 0.24v_A$ , which is the speed at which the wave front is propagating, but between A and B the phase speed increases to  $v_A$ . The reason why the wave in run 2b runs slightly faster than the wave in run 2a is that it is gaining the speed  $v_z$  of the medium in which it is propagating; a similar effect was seen in Fig. 13 of Torkelsson & Boynton (1998).

There is a gradual damping of the Alfvén wave to the left of A (Fig. 5). This decay is accompanied by a gradual

increase of the density. These changes are negligible in the low amplitude runs 2a and 3a.

The higher  $\beta$  models 3a and 3b share the characteristics of models 2a and 2b (with  $n = 5$ ), but the damping becomes more pronounced. Because of the increase in the factor  $n$ , the wave in model 3b is slower than the wave in run 2b (Fig. 6). As shown in Fig. 5b run 2b has lost  $\simeq 13.3\%$  of its Poynting flux between  $z = 0$  and point A at  $t = 133P$ . At the same time run 3b has lost  $\simeq 26.5\%$  of its Poynting flux. The stronger damping is associated with a significant modulation of the Alfvén wave on long length scales (Fig. 6)

### 3.3. $\beta = 17$

At a low magnetic pressure (runs 4a-c) the behaviour of the wave is almost independent of its amplitude. As an example we take the high amplitude model 4c with  $\eta = 0.7$ . The speed of the front of the Alfvén wave is  $\simeq 1.41v_A$  in models 4a and 4b and  $\simeq 1.43v_A$  in model 4c. The higher wave speed in run 4c is the result of that the Alfvén wave has generated an outflow with a speed  $\sim 0.02v_A$ . Analogously to models 2 and 3, the amplitude of the magnetic field has changed with a factor  $0.7 = \frac{1}{1.43}$  to compensate for the increase in the speed of the wave front (Fig. 8b). The change from sub-Alfvénic waves in runs 2 and 3 to super-Alfvénic waves in runs 4 is accompanied by a change in the character of the reflection. Fig. 7 shows that

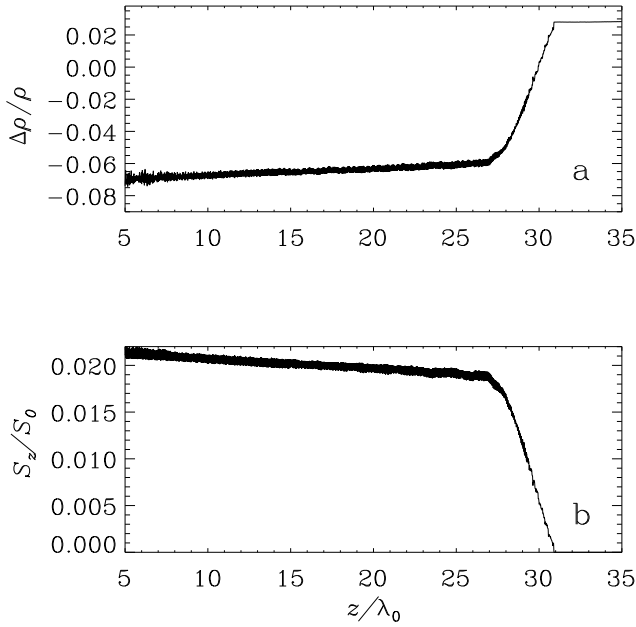


**Fig. 5.** Magnetohydrodynamic waves with  $\eta = 0.07$  propagating through a homogeneous medium of  $\beta = 0.96$  (Run 2b). **a**  $\Delta\rho/\rho = \frac{\rho - \rho_0}{\rho_0}$  versus  $z/\lambda_0$  at  $t/P = 133$ . **b** Poynting flux,  $S_z$ , versus  $z/\lambda_0$  at the same time.  $S_0$  is defined as  $v_A B_z^2/\mu_0$

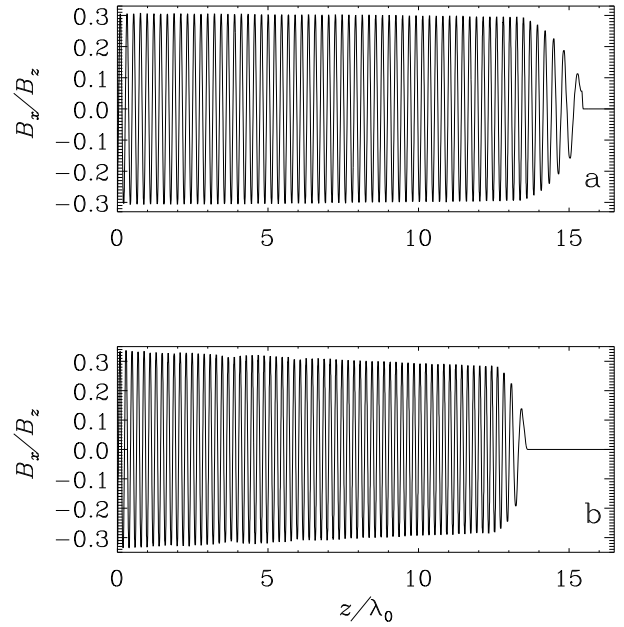


**Fig. 6.** Magnetohydrodynamic waves with  $\eta = 0.07$  propagating through a homogeneous medium of **a**  $\beta = 0.96$  (Run 2b) and **b**  $\beta = 2$  (Run 3b) versus  $z/\lambda_0$  at  $t/P = 66.7$ .

there is no phase delay between the two Elsässer variables  $z_{\pm}$ , which is a characteristic of the reflection of a wave at a free end.

Fig. 8 shows the behavior of the wave close to the reflection zone. As in models 2 and 3, the slope in density becomes less steep with time (compare Fig. 7a and Fig. 8a). The behaviour of the waves within this zone, in terms of the amplitude and the phase speed is similar to that described in sect. 3.2 for models 2 and 3 (with  $n = 1.43$ ). The difference is that the damping of the Alfvén wave outside the reflection zone is too small to be measured.

#### 4. Discussion

In constructing models of Alfvén wave driven stellar winds, it is important to understand the mechanism by which the Alfvén waves are damped. A linearly polarised Alfvén wave of high amplitude can steepen and form current sheets even in a homogeneous medium, which leads to a quick damping of the wave. While circularly polarised Alfvén waves cannot steepen in this way, they can be subject to a parametric decay into a backward propagating magnetic wave and a forward propagating density wave. Our simulations show that the compression of the background medium that takes place at the wave front of an Alfvén wave in a low  $\beta$  plasma is sufficient to trigger this instability. At  $\beta \gtrsim 1$  this is not sufficient to trigger the parametric decay, but instead we find that the Alfvén wave

is reflected at the wave front, whose speed deviates from the Alfvén speed.

One can find a large range of  $\beta$ s in the solar corona and solar wind. Typically  $\beta \ll 1$  in the lower solar corona, and  $\beta \gtrsim 1$  in the solar wind (Gary 2001). This means that different processes may affect Alfvén waves in different parts of the solar corona/wind. The parametric decay should be at work in the lower solar corona, and in the presence of sufficiently large fluctuations it may also be at work in the solar wind as indicated by the numerical simulations of Del Zanna et al. (2001). Therefore either the parametric decay or reflection at the wave front may be the source of the inward propagating Alfvén waves that have been detected in the solar corona (e.g. Bavassano et al. 2000).

An interesting property of the parametric decay is that it is relatively weak at the wave front, but the backward propagating Alfvén wave that is generated serves as a seed for the instability further upstream, where the growth rate therefore becomes larger. The area close to the wave front is therefore not significantly affected by the parametric decay, though the decay becomes strong some distance behind the wave front. This gives rise to a self-limitation of the length of an Alfvén wave packet, and it also suggests that, at least in a low- $\beta$  plasma, the Alfvén wave is the least turbulent right behind the wave front. In a high- $\beta$  plasma on the other hand one may expect to see a gradual change in density right behind the wave front, and further upstream only oscillations around a constant density.

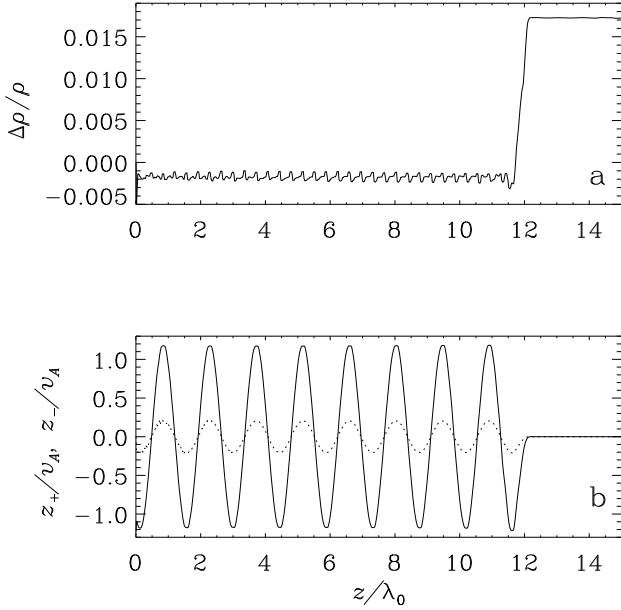


**Fig. 7.** Magnetohydrodynamic waves with  $\eta = 0.7$  propagating through a homogeneous medium of  $\beta = 17$  (Run 4c). **a**  $\Delta\rho/\rho = \frac{\rho - \rho_0}{\rho_0}$  versus  $z/\lambda_0$  at  $t/P = 33$ . **b**  $z_+/v_A$  (solid line),  $z_-/v_A$  (dotted line) and  $v_x/v_A$  (dashed line) versus  $z/\lambda_0$  at the same time.

## 5. Conclusions

In this paper we have presented numerical simulations of Alfvén waves in homogeneous media with different magnetic field strengths. In a strongly magnetised plasma the Alfvén wave decays parametrically to a backward propagating Alfvén wave and a forward propagating acoustic wave unless the amplitude of the Alfvén wave is very low. However by its very nature the parametric decay is fairly inefficient at the wave front, even when it is the cause of a strong damping upstream.

For  $\beta \sim 1$  or higher we find a different pattern. The wave front is propagating at the speed  $v_A/n$  and the magnetic field fluctuations are amplified by a factor  $n$ .  $n > 1$  for  $\beta \sim 1$  but  $n < 1$  for  $\beta \gg 1$ . At the wave front the Alfvén wave is reflected by an extended region with a positive density gradient. The spatial extent of this region increases with time. Inside this region the phase speed of the Alfvén wave is increasing from  $v_A/n$  to  $v_A$ . When  $n > 1$  the reflected Alfvén wave is phase-shifted by  $\pi$ , while it does not suffer any phase-shift for  $n < 1$ . There is also a significant gradual damping,  $\sim 10 - 20\%$  of the Alfvén wave when  $n > 1$ .

The results presented in this paper are derived from a highly simplified model, which allows us to isolate a few physical effects and study them in detail. This study can guide us in future investigations of the dynamics of Alfvén waves in more realistic configurations. In forthcoming papers we will discuss the effects of stratification and an expanding magnetic field.

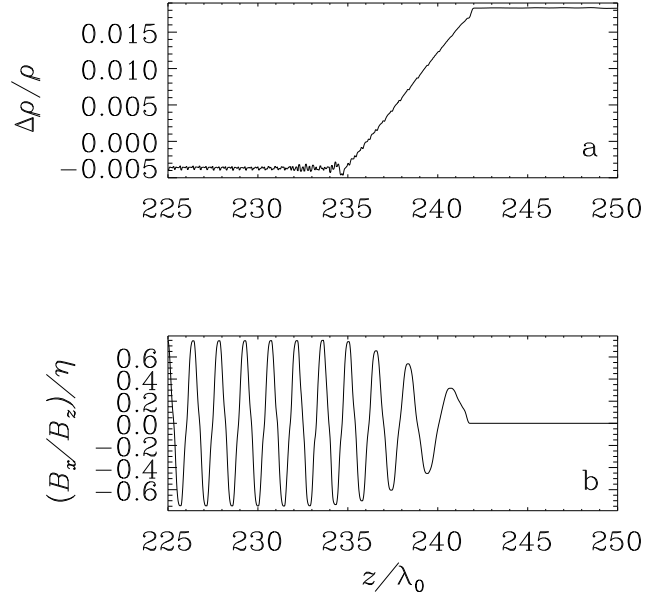


**Fig. 8.** Magnetohydrodynamic waves with  $\eta = 0.7$  propagating through a homogeneous medium of  $\beta = 17$  (Run 4c). **a**  $\Delta\rho/\rho = \frac{\rho - \rho_0}{\rho_0}$  versus  $z/\lambda_0$  at  $t/P = 169$ . **b**  $(B_x/B_z)/\eta$  versus  $z/\lambda_0$  at the same time.

*Acknowledgements.* This research was sponsored by the Swedish Research Council. RT wants to thank the solar MHD group at St. Andrews for hospitality during a part of this work. UT and RT thank UKAFF, University of Leicester for hospitality during the completion of this paper. The visitor's programme at UKAFF is sponsored by the EU Fifth Framework Programme.

## References

- Alfvén, H., & Fälthammar, C.-G. 1963, *Cosmical electrodynamics*. Fundamental principles, Clarendon Press, Oxford
- Bavassano, B., Pietropaolo, E., & Bruno, R. 2000, *JGR*, 105, 15959
- Belcher, J. W. & Davis, L. 1971, *JGR*, 79, 4174
- Boris, J. P. 1976, *NRL Mem. Rep. 3237*, Naval Research Laboratory, Washington, D.C.
- Boris, J. P., Book, D. L. 1973, *J. Comp. Phys.*, 11, 38
- Boynton, G. C., & Torkelsson, U. 1996, *A&A*, 308, 299
- Cohen, R. H., & Kulsrud, R. M. 1974, *Phys. Fluids*, 17, 2215
- Cohen, R. H. 1975, *JGR*, 80, 3678
- Cramer, N., F. 2001, *The physics of Alfvén waves*, Wiley-VCH, Berlin
- Del Zanna, L., Velli, M., & Londrillo, P. 2001, *A&A*, 367, 705
- Derby, N. F., Jr. 1978, *ApJ*, 224, 1013
- Galeev, A. A., & Oraevskii, V. N. 1963, *Sov. Phys. Dokl.*, 7, 988
- Gary, G. A. 2001, *Sol. Phys.*, 203, 71
- Ghosh, S., & Goldstein, M. L. 1994, *JGR*, 99, 13351
- Ghosh, S., Vinas, A. F., & Goldstein, M. L. 1994, *JGR*, 99, 19289
- Goldstein, M. L. 1978, *ApJ*, 219, 700
- Heyvaerts, J., & Priest, E. R. 1983, *A&A*, 117, 220



- Holzer, T. E., Flå, T., & Leer, E. 1983, ApJ, 275, 808
- Jayanti, V., & Hollweg, J. V. 1993, JGR, 98, 19049
- Landau, L. D., & Lifshitz, E.M. 1987, Fluid Mechanics, Pergamon Press, Oxford
- Laveder, D., Passot, T., & Sulem, P. L. 2002a, Phys. Plasma., 9, 293
- Laveder, D., Passot, T., Sulem, P. L. 2002b, Phys. Plasma., 9, 305
- Leer, E., Holzer, T. E., & Flå, T. 1982, Space Sci. Rev., 33, 161
- Malara, F., Primavera, L., & Veltri, P. 2000, Phys. Plasma, 7, 2866
- Malara, F., & Velli, M. 1996, Phys. Plasma, 3, 4427
- Ofman, L., & Davila, J. M. 1997, ApJ, 476, 357
- Parker, E. N. 1958, ApJ, 128, 664
- Pruneti, F., & Velli, M. 1997, in Proceedings of the Fifth SOHO Workshop: The Corona and Solar Wind Near Minimum Activity, ESA SP-404, 623
- Sagdeev, R. Z., & Galeev, A. A. 1969, Nonlinear Plasma Theory, Benjamin, New York
- Smith, E. J., Balogh, A., Neugebauer, M., & McComas, D. 1995, GRL, 22, 3381
- Torkelsson, U., & Boynton, G. C. 1998, MNRAS, 295, 55
- Tsiklauri, D., & Nakariakov, V. M. 2002, A&A, 393, 321
- Tsiklauri, D., Nakariakov, V. M., & Arber, T. D. 2002, A&A, 395, 285
- Tu, C., -Y., & Marsch, M. 1989, JGR, 95, 4337
- Umeki, H., & Terasawa, T. 1992, JGR, 97, 3113
- Wentzel, D. G. 1973, Sol. Phys., 39, 129